

Magnetic frustration on the diamond lattice of the A-site magnetic spinels $\text{CoAl}_{2-x}\text{Ga}_x\text{O}_4$: The role of lattice expansion and site disorder

Brent C. Melot, Katharine Page and Ram Seshadri
*Materials Department and Materials Research Laboratory
University of California, Santa Barbara CA 93106*

E.M. Stoudenmire and Leon Balents
*Department of Physics,
University of California, Santa Barbara, CA 93106*

Doron L. Bergman
*Department of Physics, Yale University
P.O. Box 208120, New Haven, CT 06520-8120*

Thomas Proffen
*Los Alamos National Laboratory, Lujan Neutron Scattering Center
LANSCE-12, MS H805, Los Alamos, NM 87545*

The spinels CoB_2O_4 with magnetic Co^{2+} ions on the diamond lattice A site can be frustrated because of competing near-neighbor (J_1) and next-near neighbor (J_2) interactions. Here we describe attempts to understand these interactions by substitution on the non-magnetic B-site. The system we employ is $\text{CoAl}_{2-x}\text{Ga}_x\text{O}_4$, where Al is systematically replaced by the larger Ga, ostensibly on the B site. Ga substitution has the effect of expanding the lattice and pushes Co atoms on the A-site further away from one another weakening the magnetic interactions. We also find, however, that Ga distributes between the B and the A site in a concentration dependent manner displacing an increasing amount of Co from the A site for larger values of x . This site mixing, confirmed by powder neutron diffraction studies carried out at room temperature, affects magnetic properties very significantly and changes the nature of the ground state. We discuss the role that both structural changes play in changing the degree of magnetic frustration on the diamond lattice. We also use classical Monte-Carlo modeling of the magnetic coupling to illustrate the complexity of the interactions that arises from site mixing.

PACS numbers: 75.50.Ee, 75.40.Mg,

I. INTRODUCTION

The presence of magnetic frustration in the solid state is known to give rise to multiple, nearly degenerate and often non-collinear magnetic ground states.^{1,2,3} Interest in the competition between these ground states has attracted considerable attention in recent years with the resurgent field of multiferroics: systems with spiral spin ordering are known to couple spin and lattice degrees of freedom^{4,5,6} and in specific cases, to even give rise to spontaneous polarization.^{7,8}

One highly studied class of materials that has been shown to exhibit this type of non-collinear ordering resulting from magnetic frustration is the spinel family.^{9,10} Spinel has the general formula AB_2X_4 , and in so-called normal spinels, the A site is divalent and tetrahedrally coordinated by the anion X, while the B site is trivalent and octahedrally coordinated by the anion X (typically O or S). Both sites can accommodate magnetic cations allowing for a wide range of magnetic properties. It is important to note that these sites are often not well ordered and as a consequence it is frequently appropriate to write the formula as $(\text{A}_{1-\delta}\text{B}_\delta)(\text{A}_\delta\text{B}_{2-\delta})\text{X}_4$ where δ is referred to as the inversion parameter and can be any

value $0 \leq \delta \leq 1$.

The spinel structure can be viewed as two interpenetrating sublattices with B atoms forming a pyrochlore lattice while the A atoms constitute a diamond lattice.¹¹ It is well known that there are multiple magnetic interactions in these systems. Here we focus mostly on the nearest neighbor (J_1) and next nearest neighbor (J_2) exchange interactions on the diamond lattice using the compound CoAl_2O_4 as a starting point (Fig. 1). Since the diamond lattice can be broken down further into two interpenetrating face-centered cubic (*fcc*) sublattices, we can envisage J_1 as coupling the two *fcc* sublattices to each other and J_2 coupling nearest neighbors within each sublattice.¹²

In a recent work Tristan *et al.* demonstrated that normal spinels, $\delta \ll 1$, with magnetic cations on the A site and non-magnetic cations on the B site can exhibit strong magnetic frustration.¹³ These A-site magnetic spinels have been studied in the past by Roth¹⁴ and Blasse.¹⁵ Recent modelling studies by Bergman *et al.* suggested that the magnitude of the ratio J_2/J_1 can strongly influence the dominant magnetic ground state in these systems.¹² In the limit that $J_2/J_1 \approx 0$, the magnetic ordering is a simple Néel state (magnetically speak-

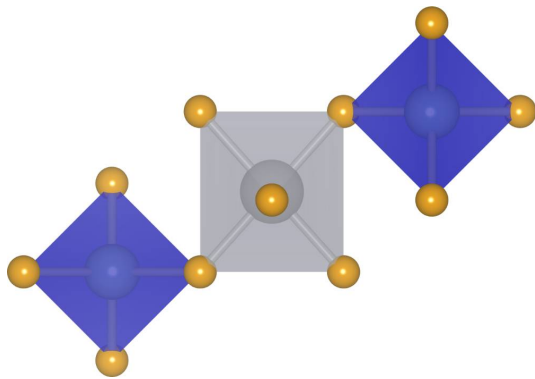


FIG. 1: (Color online) Illustration of the superexchange pathway for magnetic interactions between neighboring A-site atoms in the AB_2O_4 spinel structure. A atoms are blue (dark grey), B are light grey (light grey) and O are the orange (grey) spheres. Note that the near-neighbor J_1 coupling proceeds from each A atom to one of its 4 near-neighbor A atoms through this 6-fold degenerate pathway. The next-near-neighbor J_2 coupling to one of the 12 next-near neighbors is doubly degenerate and proceeds through an identical pathway.

ing, a diamond to zinc blende transition). As the ratio becomes larger, the nature of the magnetic ground state can change from Néel to a complex spiral pattern with the spirals oriented parallel to (111) planes. Tristan *et al.*¹⁶ have also recently examined solid solutions between $CoAl_2O_4$ and Co_3O_4 to investigate the effect of the B site cation in the superexchange pathways that connects neighboring A sites.

These recent studies have encouraged us to attempt to alter this ratio of J_2/J_1 in these A-site magnetic spinels by controlling interatomic spacings through appropriate substitution on the B site of the spinel structure. We use Ga substitution ostensibly on the B site of spinels $CoAl_{2-x}Ga_xO_4$ as a means of separating the Co from one another, given that Ga^{3+} is significantly larger than Al^{3+} (the respective 6-coordinate radii are 0.62 Å and 0.535 Å).¹⁷ We find that while the effect of such substitution is indeed to steadily increase the distance between neighboring Co atoms, there is the additional effect that site inversion in the structure steadily increases simultaneously. While separating the effects of these simultaneous changes in the structure is difficult, we discuss the role each change plays in the context of the altered frustration parameter.

II. EXPERIMENTAL DETAILS

Polycrystalline samples of the compounds were prepared using ceramic routes. Cobalt oxalate ($CoC_2O_4 \cdot 2H_2O$) was mixed with stoichiometric amounts

of Ga_2O_3 and Al_2O_3 and intimately ground with ethanol in an agate mortar. The powders were then pressed into 13 mm pellets and fired in air in alumina crucibles at 800°C for 24 h. The pellets were then reground, pressed again into pellets, and fired at 1200°C (1000°C for $x=0.0$) for 12 h. In order to obtain equilibrated samples, all pellets were annealed by heating to 700°C for 12 h, cooling to 400°C at a rate of 3°C min⁻¹, soaking at 400°C for 120 h¹⁸ followed by cooling in the furnace to the room temperature. For all heat treatments, pellets were placed on a bed of powder with the same stoichiometry to minimize reaction with the crucible.

X-ray diffraction patterns were obtained using $CuK\alpha$ radiation on a Philips XPERT MPD diffractometer operated at 45 kV and 40 mA. Phase purity was determined by refining the patterns using the Rietveld method as implemented in the XND Rietveld code.¹⁹ Neutron diffraction data were collected on the neutron powder diffractometer (NPDF) at the Lujan Center at Los Alamos National Laboratory at room temperature, on samples sealed in vanadium cans.²⁰ Neutron diffraction data were refined using the Rietveld method as implemented in the EXPGUI-GSAS software suite.^{21,22} Local structures as obtained from pair distribution function (PDF) analysis of the total neutron scattering were extracted from the total scattering data using the program PDFgetN²³ and with a maximum momentum transfer $Q_{max} = 40 \text{ \AA}^{-1}$. The obtained PDFs were analyzed using the PDFGUI software package.²⁴ DC magnetization was measured using a Quantum Design MPMS 5XL SQUID magnetometer.

III. COMPUTATIONAL DETAILS

Classical Monte Carlo simulations of the magnetic behavior of the system were performed using the ALPS project's spinmc application.²⁵ A custom lattice with periodic boundary conditions was generated for each simulation run in order to allow disorder averaging. The lattice generation code first randomly selected an A site and then moved its spin to a B site, also chosen at random and independent of the position of the A site. The simulation was then run using a Heisenberg Hamiltonian with J_1 and J_2 bonds as described above, and with J_i impurity bonds connecting spins on B sites with their nearest-neighbor occupied A sites. Finally, because the typical error bars obtained from each Monte Carlo susceptibility simulation were negligible (about 1×10^{-4} relative error), the error bars plotted represent only variation due to the presence of disorder as obtained by averaging over several runs.

A numerically calculated inverse susceptibility curve was fit to the experimental curves as follows: first, using the fact that the Curie-Weiss temperature for the J_1 - J_2 - J_i model with an inversion parameter, δ , is given by

$$\Theta_{CW}/J_1 = -\frac{4S(S+1)}{3} [(1 + 3J_2/J_1)(1 - \delta)^2 + 3J_i/J_1(\delta - \delta^2)], \quad (1)$$

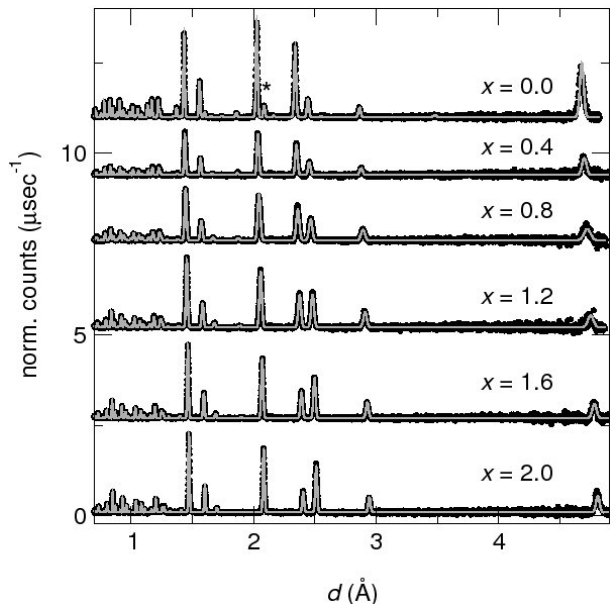


FIG. 2: Highest d -spacing bank of powder neutron diffraction data from the different samples of $\text{CoAl}_{2-x}\text{Ga}_x\text{O}_4$ collected at room temperature. Circles are data and solid lines are Rietveld fits to the spinel phase [space group $Fd\bar{3}m$, A $(\frac{1}{8}, \frac{1}{8}, \frac{1}{8})$, B $(\frac{1}{2}, \frac{1}{2}, \frac{1}{2})$, O (u, u, u)]. Asterisks denote locations where contributions to the scattering from the Al_2O_3 impurity arise.

one can calculate the value of J_1 necessary to match the experimentally measured Curie-Weiss temperature. This value of J_1 is then used to scale the temperature by a factor of $J_1 S(S+1)$ and the inverse susceptibility by a factor of $(k_B J_1 S(S+1))/(\mu_{\text{eff}}^2 \mu_B^2 N_A)$. Such a fitting procedure always guarantees that the high temperature behavior of the simulation data is in exact agreement with that of the experimental data.

IV. RESULTS

A. Structure

Rietveld analysis of the highest d -spacing bank (from four banks of data for each sample) of time-of-flight neutron diffraction data are displayed in Fig. 2 for the different spinel samples. There were no peaks in the diffraction data that could not be assigned to either the spinel phase or a small Al_2O_3 impurity in the $x = 0.0$ sample, indicating no magnetic impurities and that a complete solid solution is achieved for all values of x . The oxygen stoichiometry refined within error to the correct stoichiomet-

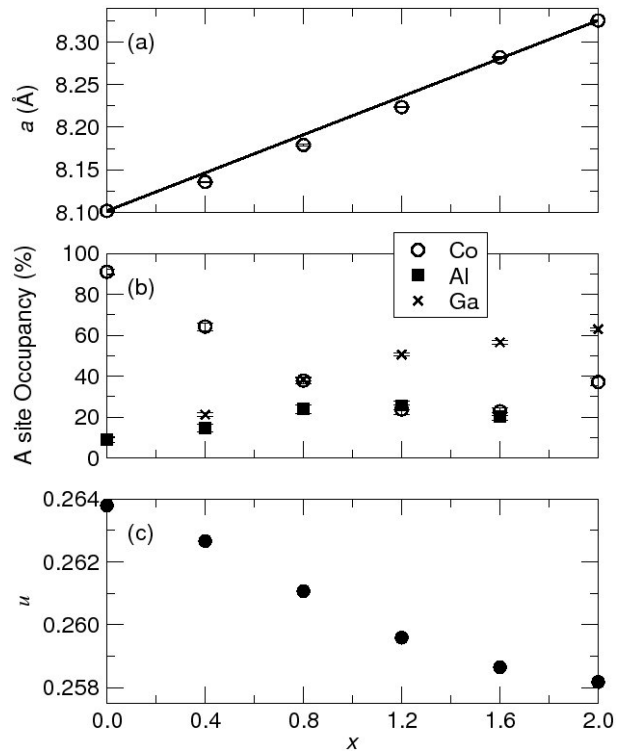


FIG. 3: Evolution of different refined structural parameters with x for the different $\text{CoAl}_{2-x}\text{Ga}_x\text{O}_4$ samples obtained from time-of-flight neutron diffraction. (a) The cell parameter, showing a nearly increase in size. The line connects end members to illustrate the Végard law. (b) Occupancies of the different cations on the A site. (c) Internal parameter u indicative of the oxygen position. $u = \frac{1}{4}$ means the BO_6 octahedra are perfectly regular.

ric value excluding the possibility that any of the Co^{2+} was oxidized to Co^{3+} . Given the close-packed nature of the oxygen lattice this was not surprising. From the Rietveld analysis, evolution of the lattice parameter, site occupancy of the cations on the A site, and the internal structural parameter (the u of oxygen) are presented in the different panels of Fig. 3. It is seen that substitution of the larger Ga^{3+} for Al^{3+} results in the spinel unit cell edge increasing from 8.1 Å to 8.3 Å. The Végard law is not strictly followed, and for all intermediate x values, the cell parameter is slightly reduced from the values suggested by a weighted average of the end-members.

Panel (b) of Fig. 3 shows the results of allowing all ions, Al, Ga, and Co to distribute themselves between the A and B sites in the refinements, with the constraint that the total amounts of the different atoms were as dictated by the starting stoichiometry. The process

of achieving this refinement involved declaring on each of the A and B sites, two separate Co atoms, one of which exchanged with Al and the other with Ga. A related procedure has been described by Joubert *et al.*²⁶ Due to the nature of multiple constraints in the refinements, errors on the occupancies are likely to be underestimated. It is noted from Fig. 3(b) that as larger amounts of Ga are substituted into the system an increasing displacement of Co from the tetrahedral site to the octahedral site occurs. While it might be expected that the Ga^{3+} ions would prefer the octahedral site based upon its large size, the amount of Ga^{3+} found on the smaller tetrahedral site steadily increases across the substitution series. In contrast Al^{3+} ions are found to remain mostly normal with a tetrahedral site occupancy never exceeding 20%. The site preference of Ga^{3+} for the tetrahedral site is in agreement with the tendency of d^{10} Ga^{3+} to adopt sp^3 hybridization. In fact, from electrostatic arguments Miller²⁷ has determined that the relative octahedral site preference of Al^{3+} and Ga^{3+} are respectively $-2.5 \text{ kcal mol}^{-1}$ and $-15.4 \text{ kcal mol}^{-1}$ with the larger number indicative of the greater octahedral preference. In contrast, Co^{2+} has a site preference energy of $-110.5 \text{ kcal mol}^{-1}$. Nakatsuka *et al.*²⁸ have conducted a recent study on the energetics of different local bonding configurations and found that replacing the relatively large Co^{2+} ($r_{tet} = 0.58 \text{ \AA}$) on the tetrahedral site with Al^{3+} ($r_{tet} = 0.39 \text{ \AA}$) results in abnormally long bond lengths which is not favored. This effect is not as pronounced when Ga^{3+} moves to the tetrahedral site given the larger radius ($r_{tet} = 0.47 \text{ \AA}$) and that the end member CoGa_2O_4 is commonly found to be almost completely inverted.²⁹ Site mixing also serves to explain the deviation from the Vegard law that is observed in Fig. 3(a).

In Fig. 3(c), the internal parameter u reflecting the position of oxygen is displayed for the different compounds in the series. It is seen that with increasing x , this value progressively decreases. Hill *et al.*³⁰ have pointed out that in normal spinels (without any inversion) this parameter u depends on the ratio R of the octahedral to tetrahedral bond lengths according to:

$$u = \frac{R^2/4 - 2/3 + (11R^2/48 - 1/18)^{1/2}}{2R^2 - 2} \quad (2)$$

The expected values for ordered CoAl_2O_4 and CoGa_2O_4 using the appropriate ionic radii¹⁷ would be respectively 0.265 and 0.261. The observed trend of a decreasing u agrees with this expectation for the normal end-members. However, we see from Fig. 3(c) that while CoAl_2O_4 , with very small inversion has an experimentally determined u value very close to what is calculated from equation 2, the value determined for CoGa_2O_4 ($u = 0.258$) is significantly smaller than suggested by equation 2. Again, we believe this discrepancy arises because of the growing inversion in the compounds as x increases.

The pair distribution functions extracted from total scattering neutron diffraction are shown for each compo-

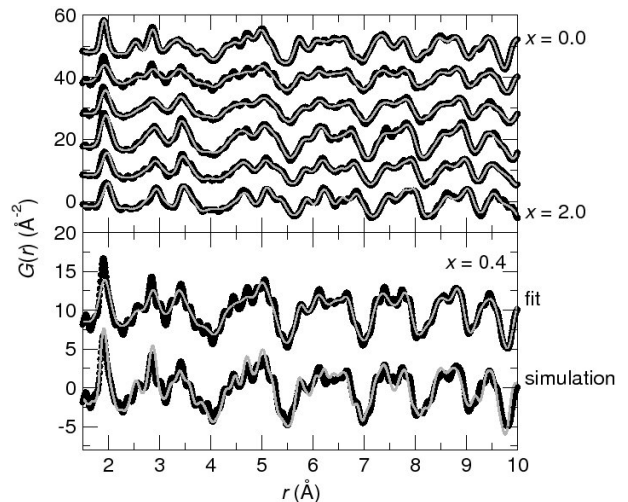


FIG. 4: (a) Neutron pair distribution functions (PDF) collected at room temperature for the different $\text{CoAl}_{2-x}\text{Ga}_x\text{O}_4$ samples with $x = 0.0$ at the top of the panel and $x = 2.0$ at the bottom. Experimental data are filled grey circles and the lines are fits obtained by refining data against the average spinel structure. (b) Experimental PDFs of the $x = 0.4$ sample (filled grey circles) compared with the refinement using the average structure (labeled “fit”) and compared with a simulation (labeled “simulation”) prepared by taking the weighted average of experimental PDFs of the $x = 0.0$ sample (80% weighting) and $x = 2.0$ (20% weighting).

sition in Fig. 4(a) along with fits (shown as lines) obtained by refining the average spinel unit cells with the appropriate site inversion. Several characteristics can be observed directly. The unit cell expansion is apparent in the movement of atom-atom peaks to longer r with increasing x . The first atom-atom peak become increasingly broad as x increases, perhaps as a result of increased site mixing, in turn resulting in a distribution of cation-oxygen distances. Furthermore, features in the intermediate compositions can be linked to the CoAl_2O_4 and CoGa_2O_4 end-member PDFs, with an increasing resemblance to the CoGa_2O_4 PDF as x increases.

Refinements in real space were carried out starting with the average structure results. A stable refinement of the site occupancies could not be achieved and values were therefore fixed to the results obtained from the Rietveld analysis of the neutron scattering data. The parameters refined in the PDF analysis include lattice parameters, isotropic atomic displacement parameters for each atomic species, a scale factor, and quadratic peak sharpening. The refinements yielded $\chi^2 < 1$ and R_{wp} less than 15% for r -ranges from 1 to 20 \AA . From the fits of the PDF displayed in Fig. 4(a), it is seen that of all the samples, only in the data corresponding to the $x = 0.0$ sample are all the peaks well described by the model. This is keeping with the fact that only in the $x = 0.0$ sample does the average spinel structure accurately describe all the local distances, since this structure has the lowest inversion and no substitution.

In Fig. 4(a), this is shown for a particular sample with $x = 0.4$. The experimental PDF is only very poorly fit in the short r region by the average structure model (labeled “fit”). Upon close inspection of the $x = 0.4$ refinement around 3 Å and 5 Å, which correspond respectively to the first and second nearest Co neighbors, there is significant splitting of the experimental peaks which is not well represented by the average structure. However, a much better description of the $x = 0.4$ sample is a stoichiometrically weighted (80:20) average of the experimental PDFs of the end members ($x = 0.0$ and $x = 2.0$) rather than as a single phase as illustrated in Fig. 4(b). In this, a resemblance to systems such as $\text{In}_{1-x}\text{Ga}_x\text{As}^{31}$ is noted wherein the alloy compositions locally follow the bonding rules of the end-member structures, and alloy PDFs can be described using weighted averages of the end members. This result of averaging end-members only holds true for distances within a unit cell (approximately 8 Å). Outside of this range the superposition model begins to fail and the average structure proves to be a good model of the data. Thus from the local structure analysis we can see that our samples have a homogeneous distribution of substituted cations and there does not seem to be any evidence for local clustering of cations.

B. Magnetism

Figure 5 displays the temperature dependence of the DC magnetic susceptibility χ of the different spinel samples on a single scaled plot. For all samples, data between 350 K and 400 K were fit with high reliability by

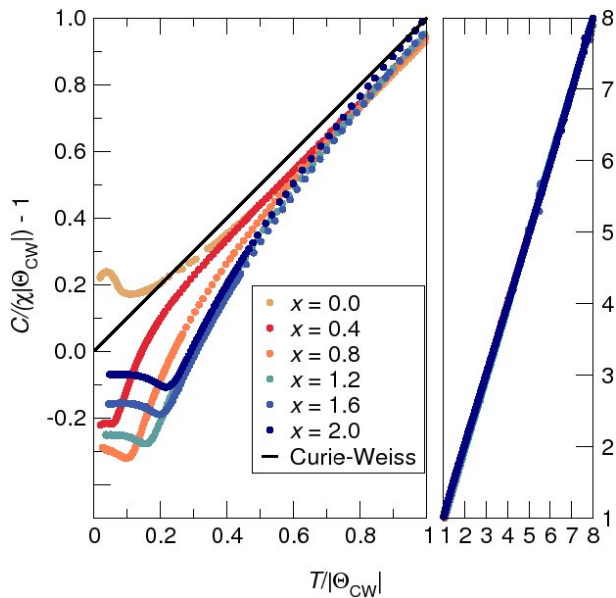


FIG. 5: (Color online) Temperature dependence of the scaled zero-field cooled magnetic susceptibility of the different spinel samples. Data were acquired under a 100 Oe field. The nature of the scaling is described in the text.

the Curie-Weiss formula: $\chi = C/(T - \Theta_{CW})$, where C is the Curie constant, and Θ_{CW} is the Curie-Weiss ordering temperature. We can recast this formula as:

$$\frac{C}{\chi|\Theta_{CW}|} = \frac{T}{|\Theta_{CW}|} - 1 \quad (3)$$

Evidence of Curie-Weiss behavior at high temperatures is seen from the right, higher temperature, panel of Fig. 5. For each sample, and at all temperatures above the individual Θ_{CW} (indicated in Table I, and approximately ranging between -100 K and -40 K) the scaled inverse susceptibility (left-hand side of equation 3) is precisely equal to $T/|\Theta_{CW}|$. All the samples order at temperatures well below $|\Theta_{CW}|$ as seen in the left-hand low-temperature panel of Fig. 5. A curious point to note is that while all the samples display a downturn in plots of χ vs. T , it is only the $x = 0.0$ sample, CoAl_2O_4 , that stays largely superior to the dotted Curie-Weiss line. The behavior of $x = 0.0$ is distinctly different from all other samples which progressively deviate from the dotted Curie-Weiss line at higher temperatures as x increases. The utility of plotting the inverse susceptibility of a solid solution in the manner shown in Fig. 5 becomes evident in the way compounds with uncompensated spins due to inversion ($x \geq 0.4$) are separated from the antiferromagnetic $x = 0.0$ end member³⁴. A plot of $1/\chi$ vs. T does not reveal this since the magnitude of the susceptibilities varies through the series.

Table I also shows values of μ_{eff} obtained from the Curie constant C for the different spinel samples. The expected spin-only value of the magnetic moment for tetrahedral Co^{2+} is $3.88 \mu_B$ whereas a value of $5.20 \mu_B$ ³⁵ is expected for systems with completely unquenched orbital contribution. The values obtained here run between $4.59 \mu_B$ and $4.85 \mu_B$, and are therefore sandwiched by the limits of the completely quenched and unquenched orbital contributions. Measured values from the literature are in the range of $4.4 \mu_B$ to $4.8 \mu_B$.³⁵ Cossee and van Arkel³⁶ have argued that for tetrahedral Co^{2+} , the proximity of a low-lying excited spin state adds a temperature-independent term to the Curie-Weiss law and that after making such a correction, magnetic moment is close to $4.4 \mu_B$. We expect CoAl_2O_4 , with a very small degree of inversion, to display a μ_{eff} value which is close to $4.4 \mu_B$. We find that for $x \neq 0$ in the substitution series, the value of μ_{eff} is always larger than for $x = 0.0$, which we attribute to the increasing amount of octahedral Co^{2+} which has a larger orbital contribution to the effective moment and correspondingly has an experimental range of μ_{eff} from $4.7 \mu_B$ to $5.2 \mu_B$.³⁵

Figure 6 shows in closer detail, the temperature dependence of the magnetic susceptibilities of the title spinel compounds at low temperatures. All the compounds display splitting of the FC and ZFC data between 4 K and 12 K. CoAl_2O_4 ($x = 0.0$) shows very little irreversibility and only a gentle downturn near 12 K. Below 4 K, there is a small upturn in the susceptibility which could arise

TABLE I: Magnetic data of different spinel compounds. Θ_{CW} is obtained from the fit to the high temperature inverse susceptibility data as described in the text. T_N is taken as the point where the ZFC and FC magnetization curves diverge with respect to temperature. f is obtained from Θ_{CW}/T_N . The inversion parameter δ is also indicated for all samples.

Compound	δ	μ_{eff} (μ_B)	Θ_{CW} (K)	T_N (K)	f	Reference
$x = 0.0$	0.09	4.59	-103	12	8.6	this work
$x = 0.4$	0.36	4.80	-96	5.3	18	
$x = 0.8$	0.62	4.83	-75	7.3	10	
$x = 1.2$	0.76	4.83	-54	8.3	6.5	
$x = 1.6$	0.77	4.80	-45	9.0	5.0	
$x = 2.0$	0.63	4.84	-42	9.2	4.6	
CoGa_2O_4	0.29	4.96	-55	10	5.5	32
CoAl_2O_4	0.04		-89	9	10	33
Co_3O_4	0.00		-110	30	3.7	33
CoRh_2O_4	0.00		-31	25	1.2	33

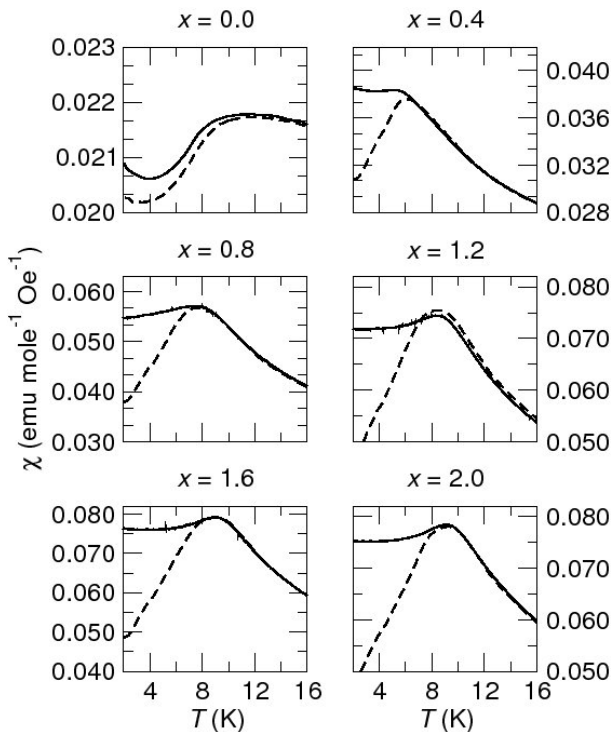


FIG. 6: Field-cooled (FC, solid) and zero-field cooled (ZFC, dashed) molar DC susceptibility of the spinel compounds at low temperatures. Data were acquired under a magnetic field of 1000 Oe.

from uncompensated spins. All other compounds with $x \geq 0.4$ show the characteristic cusps of glassy systems associated with freezing of spins and no long range order as may be expected for crystallographically disordered antiferromagnets. For all samples T_N was taken as the point of splitting between the ZFC and FC curves.

A gradual opening of the $M - H$ traces as x is increased is seen in Fig. 7 which accompanies the increasing concentration of Co atoms on the octahedral site. As

the magnetic ions enter the B site the A-B interaction begins to dominate^{15,37}, and even though both sites have the same number of spins, this interaction can give rise to uncompensated spins which could open the $M - H$ loops due to the unequal number of A and B sites. The near neighbor antiferromagnetic interaction between Co on the A and B sites, which are only separated by a single O atom will compete strongly with the pure A-A interactions where the magnetic ions are separated by $-O-B-O-$ linkages. This interaction thereby adds another competing exchange pathways which may prevent long range antiferromagnetic order between Co atoms on the tetrahedral sites from being achieved and give rise to glassy behavior instead.³⁸ It should also be noted for high enough concentrations of Co^{2+} on the B site that a ferromagnetic direct exchange between neighboring B-B atoms will begin to arise which could also give rise to the open $M - H$ loops.³⁹

For higher concentrations of Ga, it can be seen in Table I and Fig. 8 (a) that Θ_{CW} gradually decreases. Comparing the title compounds with systems that have a well ordered magnetic A lattice such as Co_3O_4 and CoRh_2O_4 shows an almost linear dependence of Θ_{CW} with respect to nearest neighbor separation d_{AA} (and correspondingly next-near neighbor A-A separation). We note that the deviation from the linear trend for samples with $x \geq 0.8$ can be understood by the site mixing in the samples reducing the number of magnetic cations on the A site. Further evidence that this the deviation from linearity is a result of site disorder is the fact that a separate report on a sample CoGa_2O_4 with half of the site mixing present in our samples lays on the line.

The structural changes also affect the temperature where the system transitions from the paramagnetic to glassy state which we take to occur where the zero field cooling and field cooling data deviate as discussed earlier (Fig. 8 (a)). For small concentrations of Ga with $x = 0.4$, a sharp drop of the transition temperature to 5 K from 10 K for the pure CoAl_2O_4 which we attribute to the sudden increase in atomic disorder and dilution

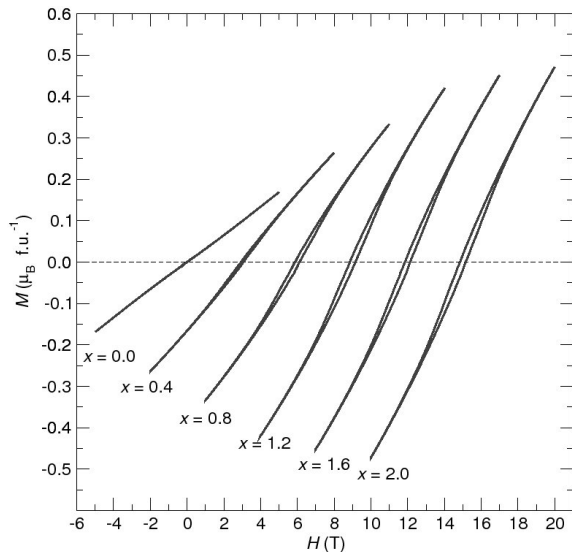


FIG. 7: Magnetization as a function of magnetic field for all samples obtained at 2 K in fields up to 5 T. Note that each curve has been shifted in 3 T increments to show more clearly the opening of the loops with increasing x .

of the magnetic A site lattice⁴⁰. This decrease is then followed by a gradual increase as more Al is replaced by Ga. Tristan *et al.* have studied the effect of replacing the Al^{3+} with non-magnetic octahedral Co^{3+} .¹⁶ It is interesting to note that changes in the non-magnetic B site cation result in little to no change in Θ_{CW} , however a clear increase in the ordering temperature is observed.

Figure 8 (b) plots the measured frustration parameter, $f = \Theta_{CW}/T_N$, as a function of d_{AA} , the separation between A ions in the different structures, including values for Co_3O_4 and CoRh_2O_4 taken from the literature. Considering the changes in Θ_{CW} and T_N we find with the exception of $x = 0.4$ the frustration index decreases systematically with increasing d_{AA} separation.

In order to better understand the behavior of the samples, we performed classical Monte Carlo simulations of the J_1 - J_2 model on the A-site spinel lattice, introducing a certain amount of inversion randomly each time a simulation run was performed. We also assumed that impurity spins occupying B sites interact with their nearest neighbors on occupied A sites via a Heisenberg exchange coupling J_i .

In Fig. 9, we show the results of a scan of various parameters. J_2/J_1 was set to 0.1, 0.2, and 0.3 while the inversion δ set to 0.0, 0.05, 0.10 and 0.20. The ratio J_i/J_1 was fixed to 1.7 throughout the scan. After plotting the resulting inverse susceptibilities in the manner described in eqn. 3, we can make a few qualitative observations. As expected, increasing J_2/J_1 increases the frustration of the system in the sense that it lowers the temperature at which evidence of ordering appears. Additionally upon introducing even a small amount of inversion, the behavior of the susceptibility below the Curie-Weiss temperature rapidly changes from antiferromagnetic (sharp up-

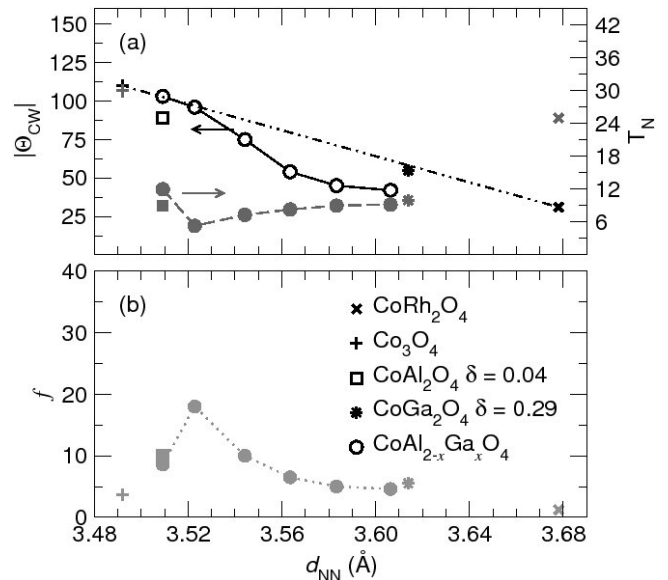


FIG. 8: (a) Curie-Weiss theta (Θ_{CW}) and ordering temperature (T_N) as a function of near-neighbor spacing between the A site atoms. The ordering temperature is taken as the point of deviation between the field cooling and zero field cooling data shown in figure 6. (b) Frustration index $f = \Theta_{CW}/T_N$ for the title compounds as a function of near-neighbor spacing between the A site atoms (d_{AA} increases with increasing Ga content, x). Also displayed is published data for CoAl_2O_4 with a different degrees of inversion: $\delta = 0.04$. By comparison, the degree of inversion of the CoAl_2O_4 sample measured in this work is close to 0.09. Values for Co_3O_4 and CoRh_2O_4 were also obtained from reference 33 while values for CoGa_2O_4 were taken from 32. Note that the values from reference 33 were not reported with lattice constants so the near-neighbor separation was taken from separate structure reports.

ward kink) to ferrimagnetic (smooth downturn) in rough qualitative agreement with the experimental results.

We also attempted to use the model to fit the individual susceptibility curves of the various experimental samples with mixed success. We first conducted simulations of the model with no inversion, in which case the fit was controlled by only one parameter, namely J_2/J_1 . These simulations were all performed on a system consisting of a cube of 64 conventional unit cells (512 spins), though for certain values of J_2/J_1 , simulations were also done using a system of 125 unit cells (1000 spins) to check for finite size effects, which were found to be negligible for the susceptibility data.

Although all of the inverse susceptibility curves produced from the numerics for the $\delta = 0.0$ case were systematically above the experimental data, they showed the correct qualitative behavior in that they exhibited an upward turning kink, presumably at the ordering temperature T_N . By increasing the value of J_2 until J_2/J_1 is around 0.15 to 0.18 (and correspondingly a J_1 between 12.1 and 12.8 Kelvin), the transition temperature T_N was brought into approximate agreement with the experimen-

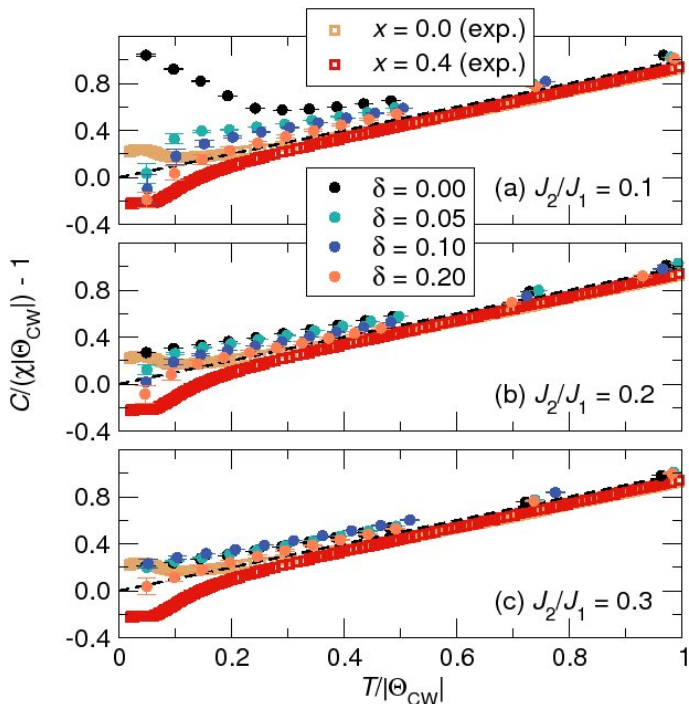


FIG. 9: (Color online) Magnetic susceptibility results from Monte Carlo simulations plotted in the form of equation 3 compared to experimental data. From top to bottom one can see the change in the shape of the low temperature susceptibility curves for increasing competition between J_2 and J_1 . Within each panel the effect of atomic disorder is shown. Note that J_i/J_1 is held constant at 1.7 for all of these simulations. The dotted line represents the expected result for a perfect Curie-Weiss system.

tally observed value as shown in Fig. 10. We also considered simulations with small amounts of inversion between 1 and 2% given that even pure CoAl_2O_4 exhibits a small amount of disorder. However, unless we ran our simulations with a value of J_i/J_1 far from the range that gave a good fit to the doped sample with $x = 0.4$ (discussed next), such a small amount of disorder changed the resulting susceptibilities very little.

We have also fit the $x = 0.4$ data by running simulations with an inversion of $\delta = 0.36$. To improve the disorder averaging, the simulations were done using a $5 \times 5 \times 5$ supercell (1000 spin) with the data presented here being the average of three independent runs. As in the case above, all of the inverse susceptibility data produced by the Monte Carlo simulations was systematically larger than the experimental curve excluding the region below the downturn. Interestingly the data could be fit equally well by a range of J_2/J_1 and J_i/J_1 values, as long as both parameters were increased together, as can be seen from Fig. 10. Since it is probably reasonable to assume that J_2/J_1 decreases slightly from the value obtained for the $x = 0.0$ sample, we can take J_2/J_1 between 0.10 and 0.15 and find that the ratio J_i/J_1 should lay between 2.0 and 2.3 whereas J_1 is found to be between 8.5 and 9.7 K.

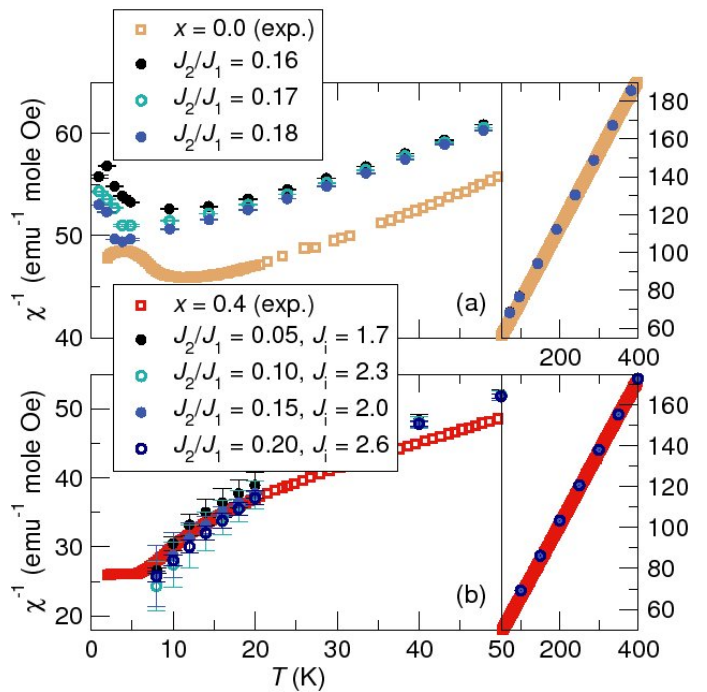


FIG. 10: (Color online) (a) Susceptibility curves obtained from Monte Carlo simulations where the effect of varying the ratio J_2/J_1 is tested in a system with no atomic disorder. (b) Susceptibility curves where the effect of varying the ratio J_2/J_1 is tested on a system with a fixed amount of atomic disorder around $\delta = 0.36$.

It is worth noting at this point that if we judge the quality of the fit in a least-squares sense, the Curie-Weiss law describes the data better than the numerical susceptibility data given that the numerical data lies above the experimental data through a wide temperature range for which a straight line fits the experimental data almost perfectly. Despite this fact, it is valuable to see that the simulation data exhibits the same qualitative low temperature behavior as the experiments. One possible explanation for the deviation between the theory and experimental data, aside from the assumption that only nearest and next nearest neighbor exchange play a role, is the possible over simplification of the g factor. One way to improve our simulations would be to allow for a temperature dependent g or also assigning a different value of g to each site.

Finally, we attempted to fit the experimental susceptibilities for the samples with $x \geq 0.8$ and were unable to obtain a good fit without changing the J_2/J_1 and J_i/J_1 by an unreasonable amount. For every set of parameters considered, the numerically calculated inverse susceptibilities exhibited strong downturns and dropped far below the experimental curve after initially matching at high temperature. Though the reasons for this negative result are somewhat unclear, it seems that either the appropriate J_2/J_1 and J_i/J_1 ratios are very far from those found above or more likely the use of only two parameters

is an over simplification considering that atomic disorder will locally modify exchange pathways and make the true exchange couplings site dependent. This possibility is supported by the PDFs presented which show the local bond lengths of the end members is retained upon substitution. Such behavior may indicate that substitution actually generates new competing J values which are not accounted for in our Monte-Carlo simulations rather than a simple modification to the existing pathways as may have been expected.

V. SUMMARY

We have attempted to understand the nature of the magnetic frustration in the A-site magnetic spinels $\text{CoAl}_{2-x}\text{Ga}_x\text{O}_4$ by substituting Ga for Al, in the hope of decreasing the relative magnetic coupling between near and next-near A atom neighbors. We have found, however, that in the compounds presented there is a significant mixing of the A and B sites in the Ga-rich samples, and this inversion has a significant influence on the magnetic coupling. The complexity of the structural changes which occur with substitution of Ga make isolating the influence of lattice expansion and site mixing a significant challenge. We have used Monte Carlo calculations

to demonstrate the importance of site mixing through a change of shape in the simulated susceptibility curves which agrees closely with our experimental findings. By comparing with samples that are perfectly ordered such as Co_3O_4 and CoRh_2O_4 , we have demonstrated that there appears to be a trend in which the frustration index f depends weakly upon the separation between magnetic ions. We have also used a variety of structural characterizations and magnetic measurements to demonstrate how both lattice expansion and site mixing can simultaneously influence the frustration parameter.

Acknowledgements

We thank A. P. Ramirez for advice in representing the magnetic data and SungBin Lee for assistance in understanding the Monte Carlo fits. We gratefully acknowledge the National Science Foundation for support through a Career Award (NSF-DMR0449354) to RS, a Graduate Student Fellowship to KP, and for MRSEC facilities (Award NSF-DMR0520415). This work has benefited from the use of NPDF at the Lujan Center at Los Alamos Neutron Science Center, funded by DOE Office of Basic Energy Sciences under DOE contract DE-AC52-06NA25396.

-
- ¹ A. Ramirez, *Annu. Rev. Mater. Sci.* **24**, 453 (1994).
 - ² J. E. Greedan, *J. Mater. Chem.* **11**, 37 (2001).
 - ³ C. J. Fennie and K. M. Rabe, *Phys. Rev. Lett.* **97**, 267602 (2006).
 - ⁴ H. Katsura, N. Nagaosa, and A. V. Balatsky, *Phys. Rev. Lett.* **95**, 057205 (2005).
 - ⁵ M. Mostovoy, *Phys. Rev. Lett.* **96**, 067601 (2006).
 - ⁶ I. A. Sergienko and E. Dagotto, *Phys. Rev. B* **73**, 094434 (2006).
 - ⁷ Y. Tokura, *Science* **312**, 1481 (2006).
 - ⁸ Y. Yamasaki, S. Miyasaka, Y. Kaneko, J.-P. He, T. Arima, and Y. Tokura, *Phys. Rev. Lett.* **96**, 207204 (2006).
 - ⁹ G. Lawes, B. Melot, K. Page, C. Ederer, M. A. Hayward, T. Proffen, and R. Seshadri, *Phys. Rev. B* **74**, 024413 (2006).
 - ¹⁰ R. Tackett, G. Lawes, B. C. Melot, M. Grossman, E. S. Toberer, and R. Seshadri, *Phys. Rev. B* **76**, 024409 (2007).
 - ¹¹ P. W. Anderson, *Phys. Rev.* **102**, 1008 (1956).
 - ¹² D. Bergman, J. Alicea, E. Gull, S. Trebst, and L. Balents, *Nature Physics* **3**, 487 (2007).
 - ¹³ N. Tristan, J. Hemberger, A. Krimmel, H.-A. K. von Nidda, V. Tsurkan, and A. Loidl, *Phys. Rev. B* **72**, 174404 (2005).
 - ¹⁴ W. L. Roth, *J. Phys. France* **25**, 507 (1964).
 - ¹⁵ G. Blasse, *Philips Res. Rept.* **18**, 383 (1963).
 - ¹⁶ N. Tristan, V. Zestrea, G. Behr, R. Klingeler, B. Büchner, H. A. K. von Nidda, A. Loidl, and V. Tsurkan, *Phys. Rev. B* **77**, 094412 (2008).
 - ¹⁷ R. D. Shannon, *Acta Crystallogr. A* **32**, 751 (1976).
 - ¹⁸ P. Porta and A. Anichini, *J. Chem. Soc. Faraday Trans.* **76**, 2448 (1980).
 - ¹⁹ J. Bézar and G. Baldinozzi, *IUCr-CPD Newsletter* **20**, 3 (1998).
 - ²⁰ T. Proffen, T. Egami, S. J. L. Billinge, A. K. Cheetham, D. Louca, and J. B. Parise, *Appl. Phys. A* **74**, S163 (2002).
 - ²¹ A. C. Larson and R. B. Von Dreele, *Los Alamos National Laboratory Report LAUR 86-748* (2000) **86**, 748 (2000).
 - ²² B. Toby, *J. Appl. Cryst.* **34**, 210 (2001).
 - ²³ P. F. Peterson, M. Gutmann, T. Proffen, and S. J. L. Billinge, *J. Appl. Crystallogr.* **33**, 1192 (2000).
 - ²⁴ C. L. Farrow, P. Juhas, J. W. Liu, D. Bryndin, E. S. Bozin, J. Bloch, T. Proffen, and S. J. L. Billinge, *J. Phys.: Condens. Matter* **19**, 335219 (7pp) (2007).
 - ²⁵ A. Albuquerque, F. Alet, P. Corboz, P. Dayal, A. Feiguin, S. Fuchs, L. Gamper, E. Gull, S. Gurtler, and A. H. *et al.*, *J. Magn. Magn. Mater.* **310**, 1187 (2007).
 - ²⁶ J.-M. Joubert, R. Cerný, M. Latroche, A. Percheron-Guégan, and K. Yvon, *J. Appl. Crystallogr.* **31**, 327 (1998).
 - ²⁷ A. Miller, *J. Appl. Phys.* **30**, 24S (1959).
 - ²⁸ A. Nakatsuka, Y. Ikeda, Y. Yamasaki, N. Nakayama, and T. Mizota, *Solid State Communications* **128**, 85 (2003).
 - ²⁹ A. Nakatsuka, Y. Ikeda, N. Nakayama, and T. Mizota, *Acta Crystallographica Section E* **62**, i109 (2006).
 - ³⁰ R. J. Hill, J. R. Craig, and G. V. Gibbs, *Phys. Chem. Minerals* **4**, 317 (1979).
 - ³¹ I.-K. Jeong, F. Mohiuddin-Jacobs, V. Petkov, S. J. L. Billinge, and S. Kycia, *Phys. Rev. B* **63**, 205202 (2001).
 - ³² D. Fiorani and S. Viticoli, *Sol. State Comm.* **25**, 155 (1978).
 - ³³ T. Suzuki, H. Nagai, M. Nohara, and H. Takagi, *J. Phys.: Condens. Matter.* **19**, 145265 (2007).
 - ³⁴ B. C. Melot, J. E. Drewes, R. Seshadri, E. M. Stoudenmire,

- and A. P. Ramirez, *J. Phys.: Condens. Matter* **21**, 216007 (2009).
- ³⁵ M. C. Day and J. Selbin, *Theoretical Inorganic Chemistry* (Reinhold Book Corporation, 1960), 2nd ed.
- ³⁶ P. Cossee and A. E. van Arkel, *J. Phys. Chem. Solid.* **15**, 1 (1960).
- ³⁷ C. Ederer and M. Komelj, *Physical Review B (Condensed Matter and Materials Physics)* **76**, 064409 (pages 9) (2007).
- ³⁸ J. Soubeyroux, D. Fiorani, and E. Agostinelli, *J. Magn. Magn. Mater.* **54-57**, 83 (1986).
- ³⁹ S. Diaz, S. de Brion, G. Chouteau, B. Canals, V. Simonet, and P. Strobel, *Phys. Rev. B* **74**, 092404 (2006).
- ⁴⁰ K. Binder and A. P. Young, *Rev. Mod. Phys.* **58**, 801 (1986).